Supplementary material

Breath-Fig.-Derived Porous Hybrid Layers for Safety-Enhanced Separators in Lithium-Ion Batteries

Yeong Hun Jeong[a], Jae Bin Park[b], Min Seo Jo[a], Sinyoung Seo[a], Da-Sol Kwon[c,d], Jin Hong Lee[b*], Jimin Shim[a*]

[a]Department of Chemistry Education, Seoul National University, Seoul 08826, Republic of Korea

[b]School of Chemical Engineering, Pusan National University, 2, Busandaehak-ro 63beon-gil, Geumjeong-gu, Busan 46241, Republic of Korea

[c]Department of Chemical and Biological Engineering, Korea University, 145 Anam-ro, Seongbuk-gu, Seoul 02841, Republic of Korea,

[d]Energy Storage Research Center, Korea Institute of Science and Technology (KIST), 14 Gil 5 Hwarang-ro, Seongbuk-gu, Seoul 02792, Republic of Korea

***Corresponding Author:** jinhong.lee@pusan.ac.kr (J. H. Lee) & jiminshim@snu.ac.kr (J. Shim)

Table S1. Raw parameters for the calculation of Li^+ transference number (t_{Li^+}) derived from chronoamperometry and EIS measurements for PE and PVB@PE separators.

Separator	I_0 (mA)	I_{ss} (mA)	R_0 (Ω)	R_{ss} (Ω)	t_{Li^+}
PE	0.112	0.092	90.0	101.5	0.36
PVB@PE	0.108	0.094	60.0	61.5	0.73

Table S2. Comparison of ionic conductivity, transference number, and Li^+ conductivity of the PVB@PE with previously published works.

Separators	Ionic conductivity (mS cm^{-1})	Transference number (t_{Li^+})	Li^+ conductivity[a] (mS cm^{-1})	Ref.
PE	0.34	0.36	0.12	This work
PVB@PE	0.75	0.73	0.54	
LSO-SiO_2@PE	0.41	0.41	0.17	R1[1]
PEAO-LTO	0.72	0.61	0.44	R2[2]
PVDF/ZSM-Si (Al)@PE	0.54	0.44	0.24	R3[3]
PEI-PSS-PLLgPEG	0.67	0.42	0.28	R4[4]

[a]Li^+ conductivity was calculated as the product of ionic conductivity and t_{Li^+}.

Table S3. Comparison of thermal stability and SET of the PVB@PE with previously published works.

Separators	Thermal stability (°C)	SET (s g^{-1})	Ref.
PE	130	410	This work
PVB@PE	150	9.9	
PP/(PVDF-HFP/MPP)	150	20	R5[5]
MT31/PE	130	133	R6[6]
PDA@mAl_2O_3-PE	150	50	R7[7]
F/PI	160	19	R8[8]

Table S4. Comparative summary of key physical and electrochemical properties for PE, PVB@PE (non-porous), and PVB@PE (porous) separators.

Metric	PE	PVB@PE (non-porous)	PVB@PE (porous)
Gurley number (s 100 cm^{-3} μm^{-1})	7.0	Not detected	4.2
Ionic conductivity (mS cm^{-1})	0.34	0.44	0.75
Electrolyte uptake (%)	101	108	187
SET (s g^{-1})	410	20	9.9

Table S5. Comparison of electrochemical performance and cell testing conditions of the PVB@PE with previously published works.

Separators	Symmetric Li/Li cell test		Full (or half)-cell test			
	Current density/total plating	Lifespan (h)	Cathode/ anode materials	C-rate	Lifespan (cycle)	Ref.
PVB@PE	1.0 mA cm^{-2} /1.0 mAh cm^{-2}	275	NCM811 /graphite	0.5 C	1000	This work
NS protected	1.0 mA cm^{-2} /1.0 mAh cm^{-2}	250	LFP/Li	1 C	150	R9[9]
PLL-20	0.2 mA cm^{-2} /0.1 mAh cm^{-2}	350	LFP/Li	0.2 C	100	R10[10]
PP-C20	3 mA cm^{-2} /1.0 mAh cm^{-2}	200	LFP/Li	0.5 C	400	R11[11]
APP	5.0 mA cm^{-2} /5.0 mAh cm^{-2}	350	NCM622/Li	0.5 C	200	R12[12]
BS/BC	–	–	LFP/graphite	2 C	500	R13[13]
PW@PAN	–	–	LFP/graphite	1 C	400	R14[14]
Inorganic separator	–	–	LFP/graphite	0.1 C	20	R15[15]
LFO-FS0	–	–	NMC811/ (SiO_x/G)	0.1 C	100	R16[16]

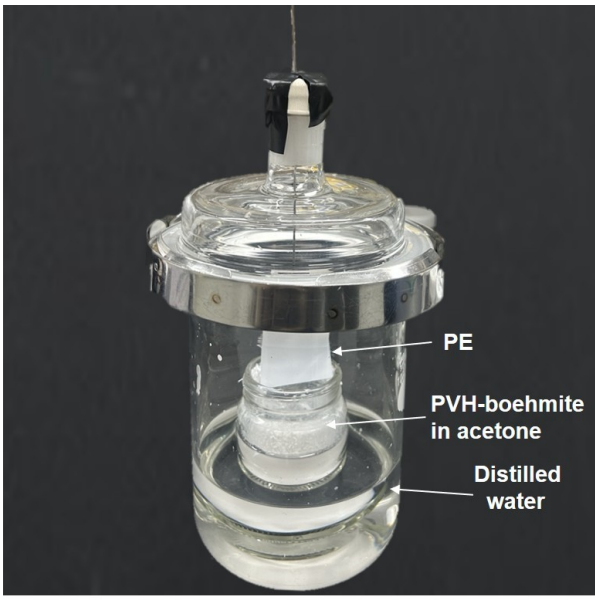

Fig. S1. Experimental setup for the static breath-Fig. self-assembly process.

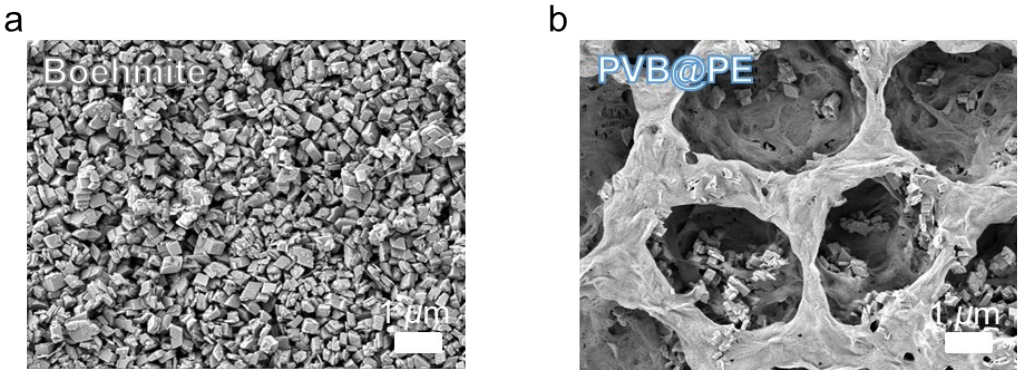

Fig. S2. SEM images of a) boehmite and b) PVB@PE.

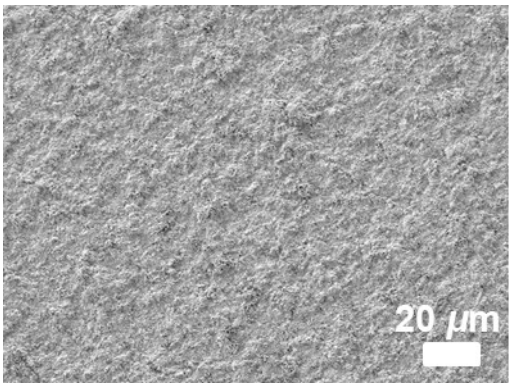

Fig. S3. Surface SEM image of nonporous PVB@PE prepared without breath-Fig. process.

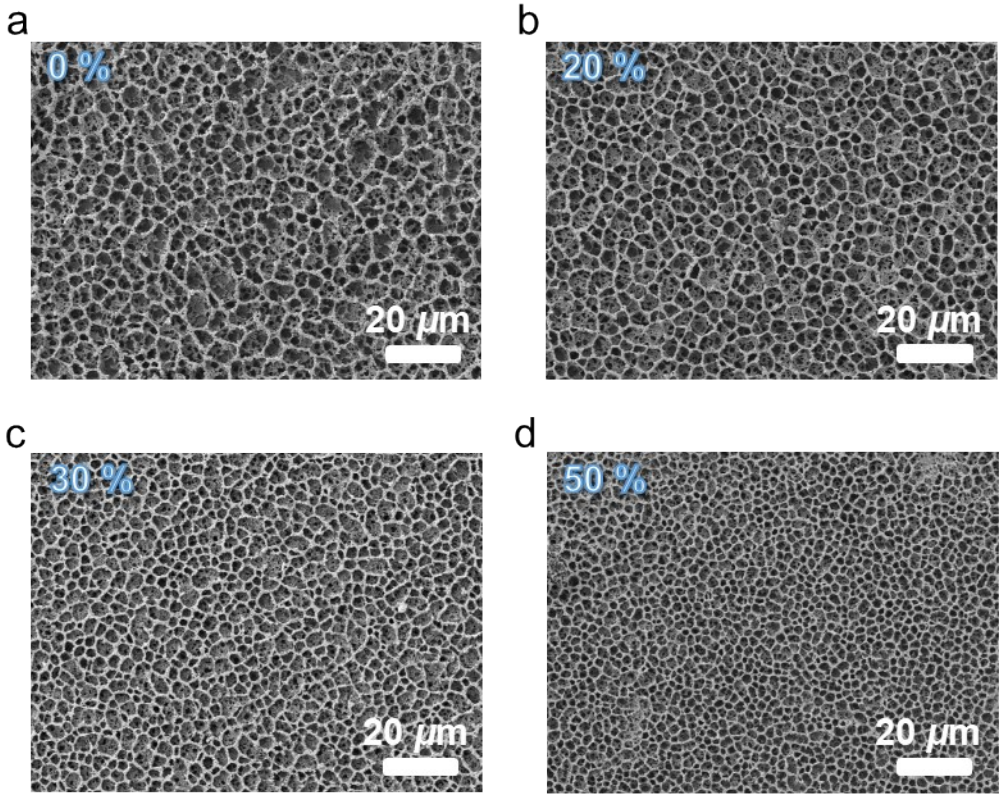

Fig. S4. Surface SEM images of PVB@PE prepared with different boehmite content: a) 0 wt% (PVH@PE), b) 20 wt%, c) 30 wt%, and d) 50 wt%.

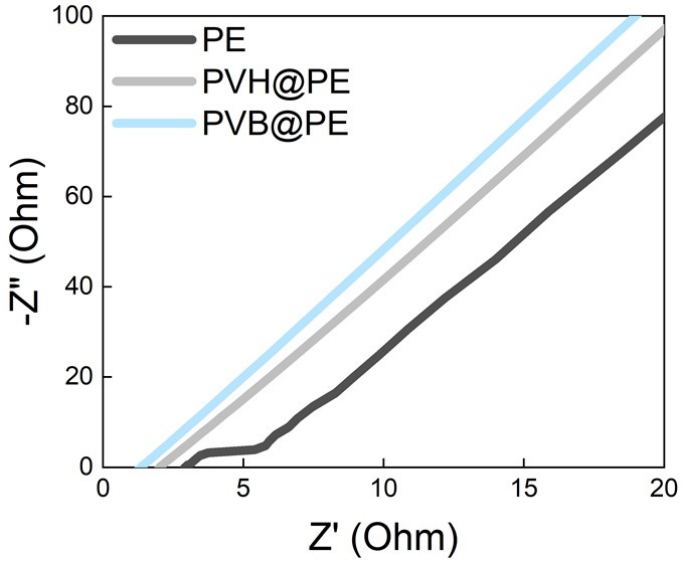

Fig. S5. Nyquist plots of PE, PVH@PE, and PVB@PE.

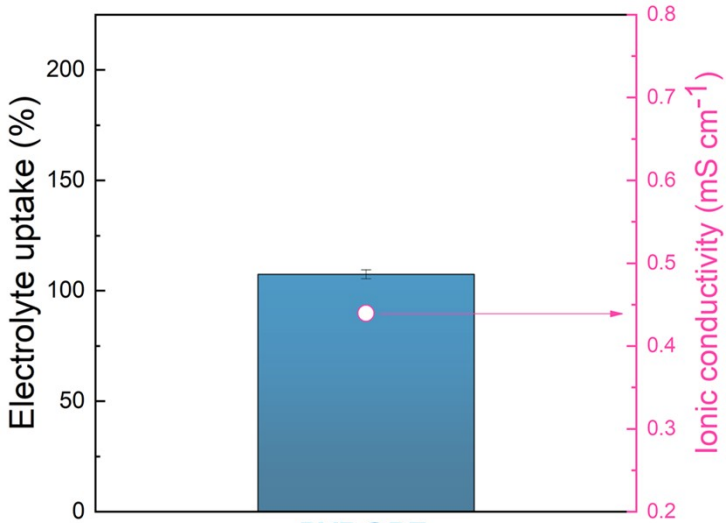

Fig. S6. Electrolyte uptake and ionic conductivity of nonporous PVB@PE.

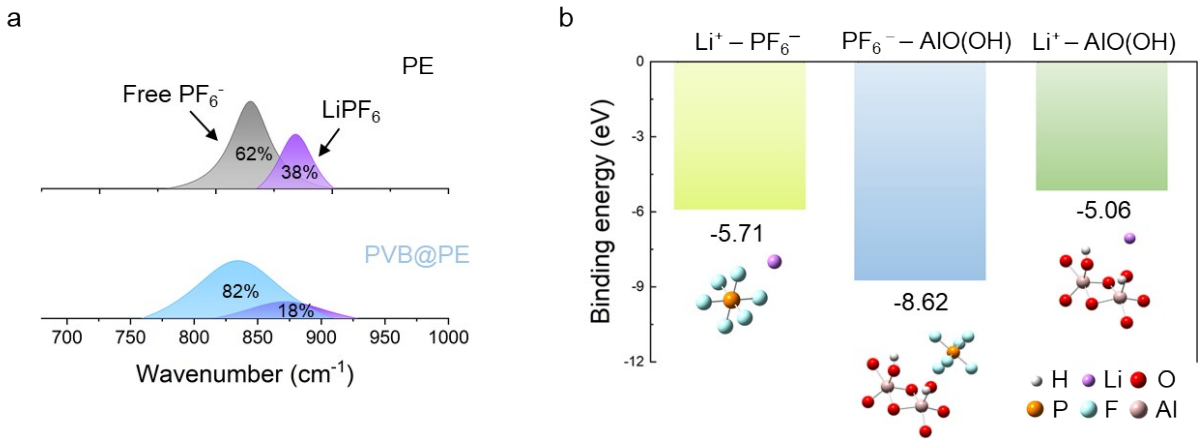

Fig. S7. a) Deconvoluted FT-IR spectra of $LiPF_6$ doped separators (at a fixed $[Li^+]/[AlO(OH)]$ ratio of 0.07) and b) DFT-calculated binding energies between Li^+, PF_6^-, and AlO(OH) surface.

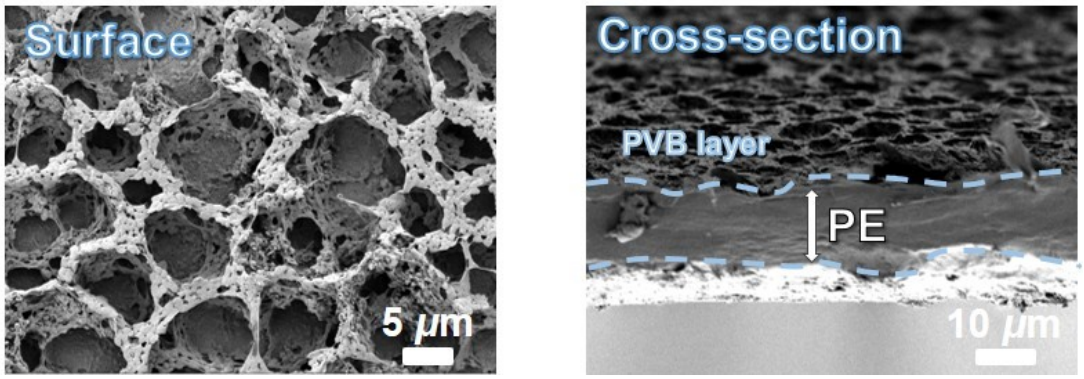

Fig. S8. Surface and cross–sectional SEM images of PVB@PE after 30 cycles of folding–unfolding fatigue testing.

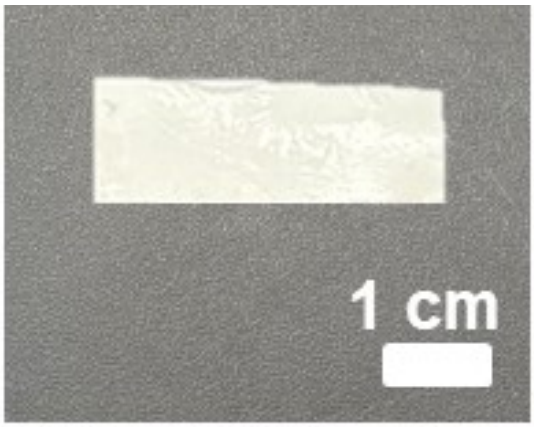

Fig. S9. Optical photograph of the adhesive tape used in the peeling test.

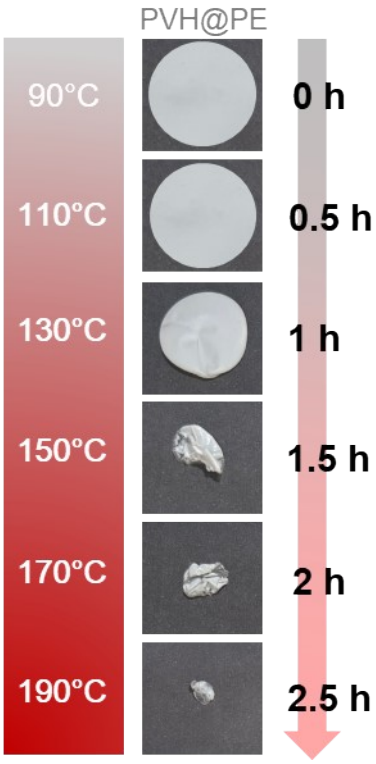

Fig. S10. Optical photographs of PVH@PE after heat treatment for 0.5 h at different temperatures.

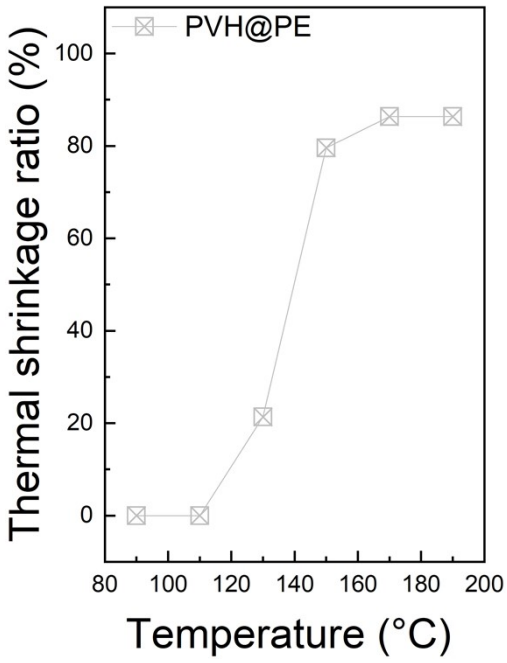

Fig. S11. Thermal shrinkage ratio of PVH@PE after heat treatment for 0.5 h at different temperatures (Thermal shrinkage ratio (%) = (S_1–S_0) / S_0 × 100), where S_0 and S_1 represent the area of the samples at the initial and final heat treatment, respectively.

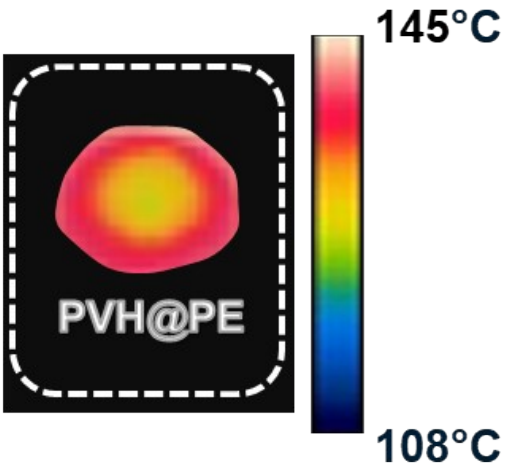

Fig. S12. Thermal infrared images of PVH@PE after heat treatment at 150 °C for 0.5 h.

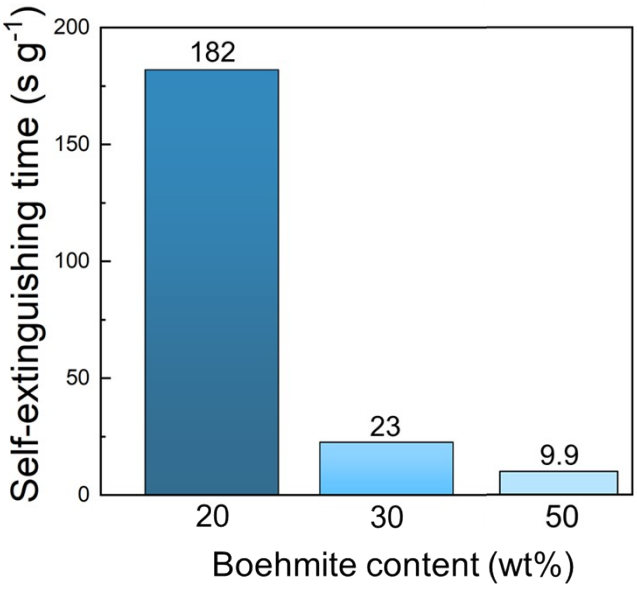

Fig. S13. SET of the PVB@PE containing different boehmite content.

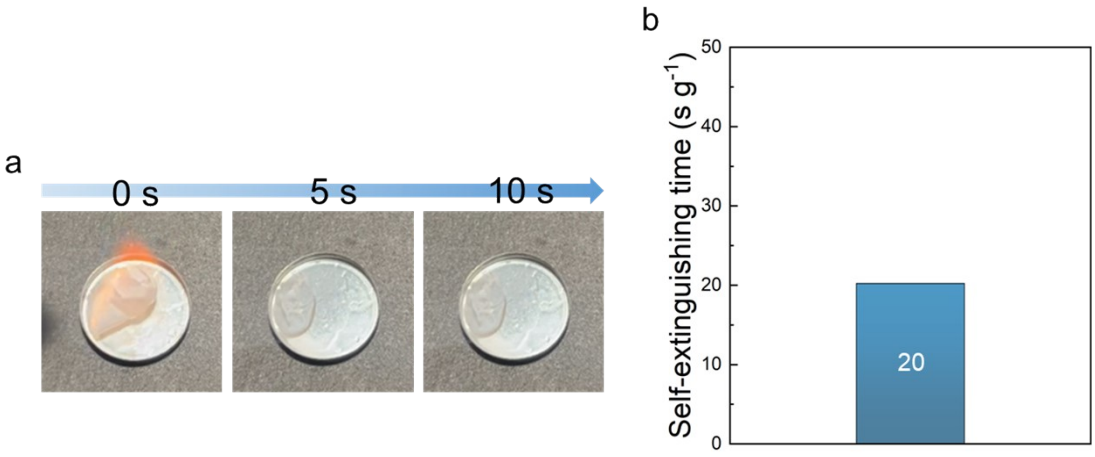

Fig. S14. a) Optical photographs during ignition tests and b) SET and weight loss percentage of nonporous PVB@PE prepared without breath–Fig. process wetted by 20 μL mg^{-1} of electrolyte.

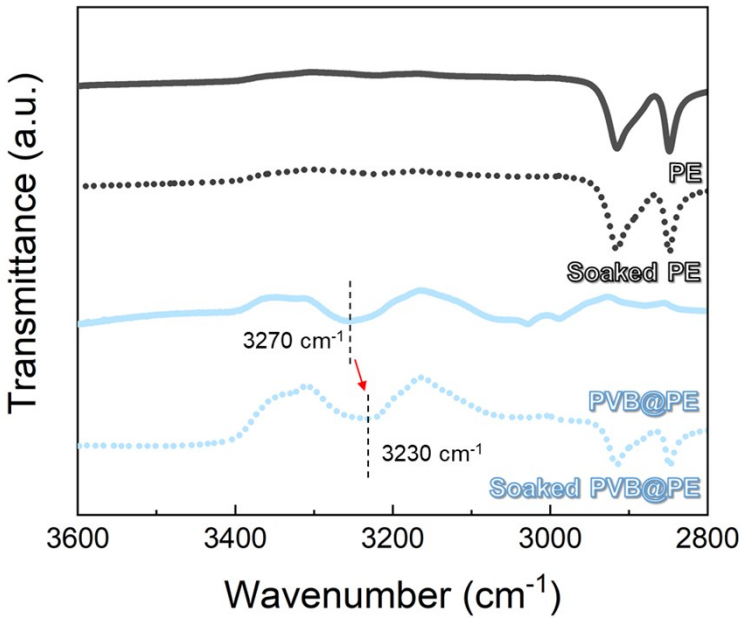

Fig. S15. FT–IR spectra of PE and PVB@PE before and after soaking in electrolyte for 24 h.

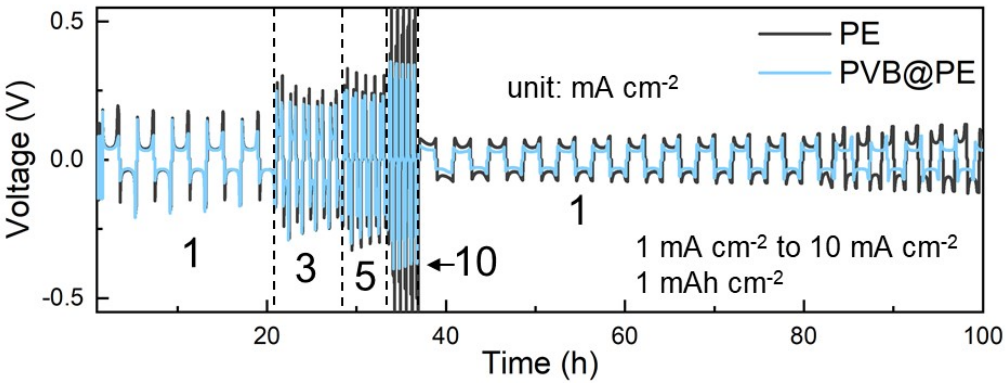

Fig. S16. Rate-dependent galvanostatic cycling profiles of symmetric Li/Li cells at current densities from 1 to 10 mA cm^{-2} with an areal capacity of 1 mAh cm^{-2} at 30 °C.

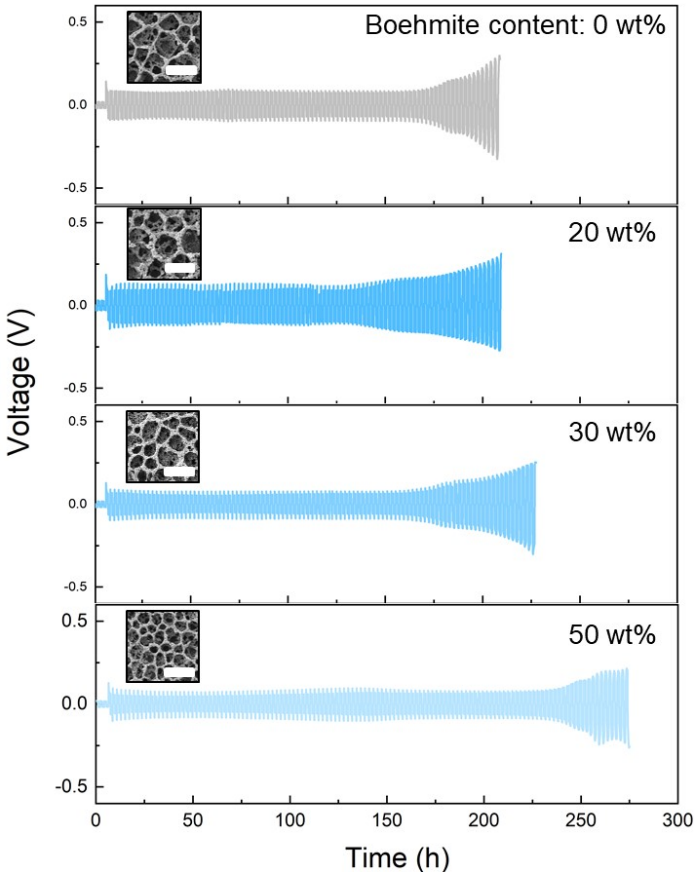

Fig. S17. Galvanostatic cycling profiles of symmetric Li/Li cells with different boehmite content: 0 wt%, 20 wt%, 30 wt%, and 50 wt% under a current density of 1.0 mA cm^{-2} and a total capacity of 1.0 mAh cm^{-2} at 30 °C. The scale bar corresponds to 10 μm.

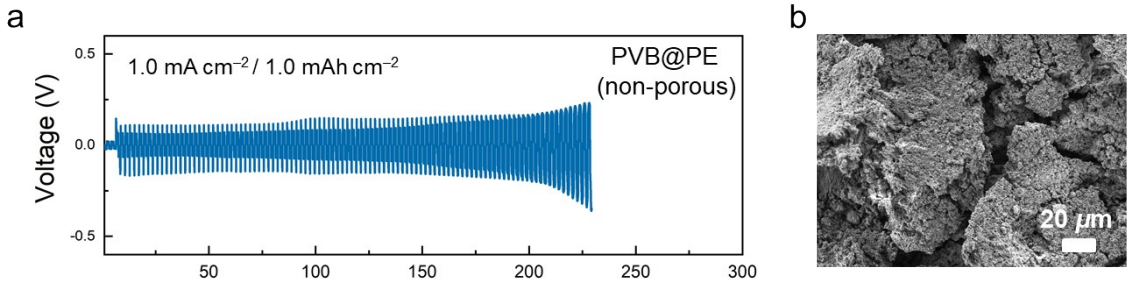

Fig. S18. a) Galvanostatic cycling profiles of symmetric Li/Li cells with PVB@PE (non-porous) under a current density of 1.0 mA cm^{-2} and a total capacity of 1.0 mAh cm^{-2} at 30 °C. The cells were subjected to formation steps cycled under a current density of 0.1 mA cm^{-2} and a total capacity of 0.1 mAh cm^{-2} for the first three cycles before the main cycling. b) Surface SEM images of cycled Li metal anodes retrieved from PVB@PE (non-porous) after the 30th cycle.

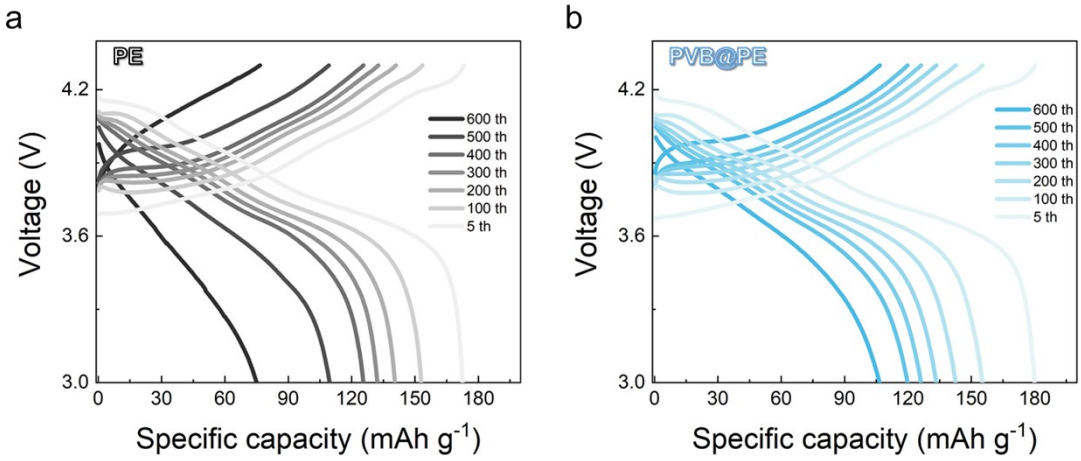

Fig. S19. Voltage–capacity profiles of a) PE and b) PVB@PE. The cycle number of the corresponding charge/discharge curves is indicated in the legend.

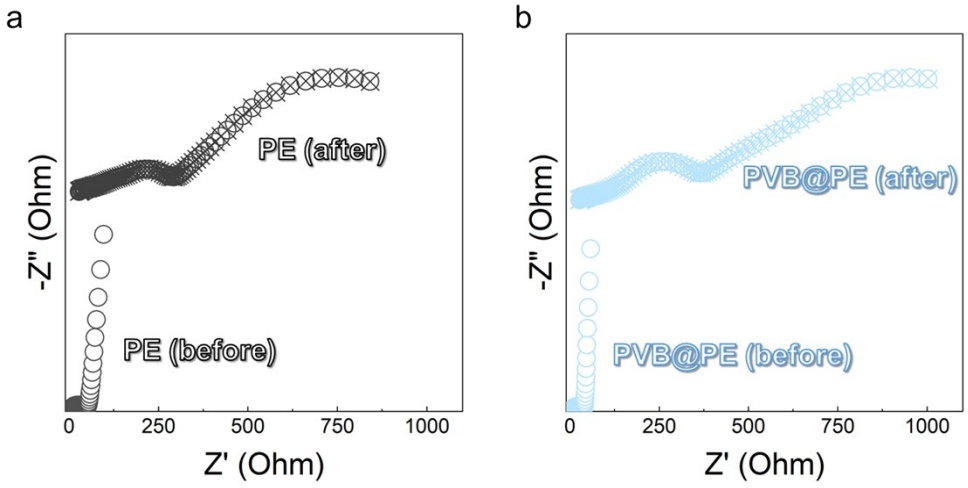

Fig. S20. Nyquist plots of the cells with a) PE and b) PVB@PE before and after cycling.

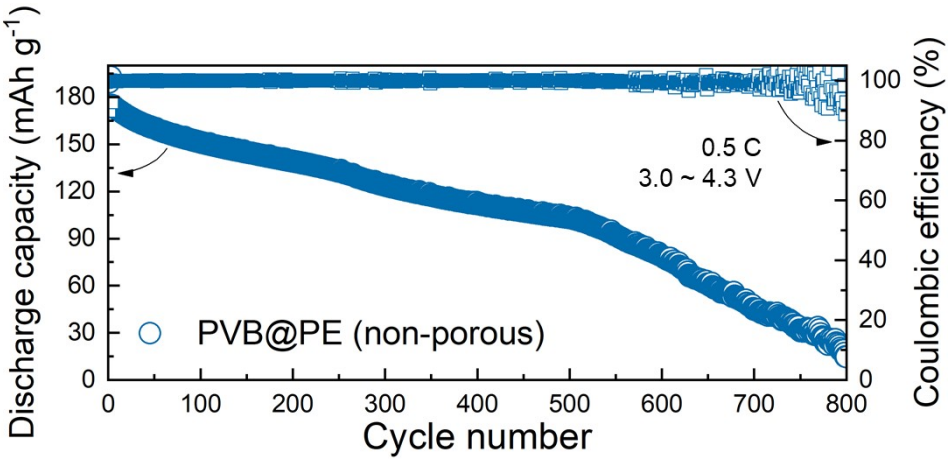

Fig. S21. Long-term half-cell cycling performance of Li/NCM811 cells with PVB@PE (non-porous) cycled under 0.5 C at 30 °C.

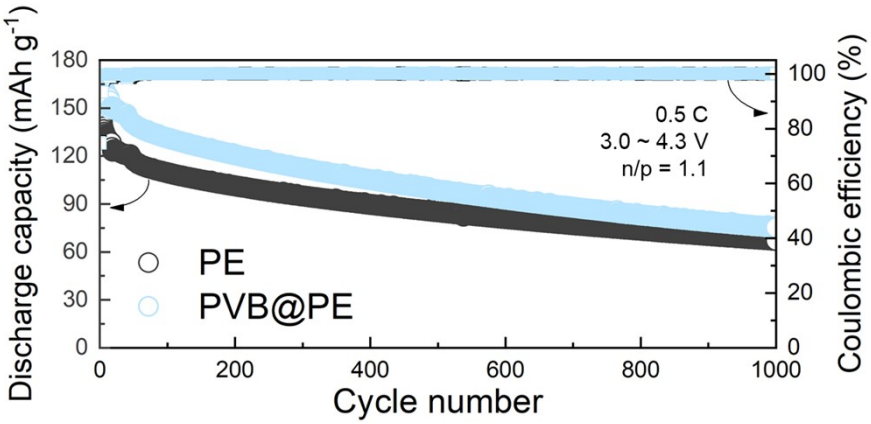

Fig. S22. Coin-type NCM811/graphite full cell cycling performance with PE and PVB@PE cycled under 0.5 C at 30 °C (mass loading: 15 mg cm^{-2}, n/p ~ 1.1).

References for Supporting Information

1 H. Zheng, Z. Wang, L. Shi, Y. Zhao and S. Yuan, *J. Colloid Interface Sci.* 2019, **554**, 29–38.
2 M. V. M. Nitou, M. Tang, Y. Niu, Y. Pang, Z. Wan, S. E. Mawuli, J. A. Leoba, F. Xiaodong and W. Lv, *ACS Appl. Mater. Interfaces,* 2024, **602**, 234406.
3 X. Mao, L. Shi, H. Zhang, Z. Wang, J. Zhu, Z. Qiu, Y. Zhao, M. Zhang and S. Yuan, *J. Power Sources,* 2017, **342**, 816–824.
4 R. Zhan, M. F. Lagadec, M. Hess and V. Wood, *J. Power Sources,* 2016, **8**, 32637–32642.
5 C. Han, Y. Cao, S. Zhang, L. Bai, M. Yang, S. Fang, H. Gong, D. Tang, F. Pan, Z. Jiang and J. Sun, *Small,* 2023, **19**, 2207453.
6 M. Hong, D. Chen, W. Zhu, G. Li, X. Zhou, W. Li and Y. Liao, *Solid State Ionics,* 2023, **19**, 116184.
7 X. Dong, T. Zhu, G. Liu, J. Chen, H. Li, J. Sun, X. Gu and S. Zhang, *J. Colloid Interface Sci,* 2023, **643**, 223–231.
8 X. Luo, X. Lu, X. Chen, Y. Chen, C. Song, C. Yu, N. Wang, D. Su, C. Wang, X. Gao, G. Wang and L. Cui, *J. Mater. Chem. A,* 2020, **8**, 14788–14798.
9 J. Liang, Q. Chen, X. Liao, P. Yao, B. Zhu, G. Lv, X. Wang, X. Chen and J. Zhu, *Angew. Chem. Int. Ed.* 2020, **59**, 6561–6566.
10 X. Fu, C. Shang, M. Yang, E. M. Akinoglu, X. Wang and G. Zhou, *J. Power Sources,* 2020, **475**, 228687.
11 X. Liang, Y. Zhou, D. Liu, H. Wang, J. Sun and X. Cai, *J. Power Sources,* 2025, **640**, 236765.
12 J. Jeong, J. Lee, J. Kim, J. Chun, D. Kang, S. M. Han, C. Jo and J. Lee, *J. Mater. Chem. A,* 2021, **9**, 7774–7781.
13 Y. Zhang, L. Chang, W.-S. Zhu, J. Wu, H.-P. Yu, S. Xie, D. Li, Z. Wang and H. Li, *J. Energy Chem.* 2021, **101**, 511–523.
14 Z. Liu, Q. Hu, S. Guo, L and X. Hu, *Adv. Mater.* 2021, **33**, 2008088.
15 H. Xiang, J. Chen, Z. Li and H. Wang, *J. Power Sources,* 2011, **196**, 8651–8655.
16 Q. Meng, M. Fan, X. Chang, W.-P. Wang, Y.-H. Zhu, J. Wan, Y. Zhao, F. Wang, R. Wen, S. Xin and Y.-G. Guo, *Adv. Energy Mater.* 2023, **13**, 2300507.